Time-dependence of the spatial pattern of accumulation rate in East Antarctica deduced from isochronic radar layers using a 3-D numerical ice flow model

Gwendolyn J.-M. C. Leysinger Vieli,[1,2] Richard C. A. Hindmarsh,[1] Martin J. Siegert,[3] and Sun Bo[4]

Received 7 June 2010; revised 13 February 2011; accepted 11 March 2011; published 11 June 2011.

[1] In East Antarctica surface mass balance data can only be obtained from the sparsely distributed ice cores when considering time periods greater than a few decades. Observations of internal layers measured by airborne ice penetrating radar, in principle, permit extrapolation of mass balance information from these ice cores. We use radar survey lines gathered in the 1970s, and a three-dimensional numerical model, to investigate the feasibility of such extrapolation, seeking to match the calculations of englacial layer geometry with observations. First, we justify the use of a three-dimensional model by showing that simple vertical flow models cannot explain all the observations and that horizontal advection is a significant glacial process. Then we examine processes that affect calculations of layer geometry, finding that spatial accumulation-rate patterns are extremely important while geothermal heat flux and flow mode (sliding or internal deformation) are of substantially less importance. Where the layer is from the Last Glacial Maximum (17.5 ka), we find a very good match between the spatial pattern of accumulation rates inferred from this layer and the modern spatial pattern of accumulation rates. When considering deeper layers from beyond the current interglacial, we find that a different spatial accumulation-rate pattern must have existed, in addition to the known change in accumulation rate from ice cores. The glacial spatial accumulation-rate pattern would have had proportionally greater accumulation at the South Pole than now, compared with the Vostok and Dome C ice cores.

Citation: Leysinger Vieli, G. J.-M. C., R. C. A. Hindmarsh, M. J. Siegert, and S. Bo (2011), Time-dependence of the spatial pattern of accumulation rate in East Antarctica deduced from isochronic radar layers using a 3-D numerical ice flow model, *J. Geophys. Res.*, *116*, F02018, doi:10.1029/2010JF001785.

1. Introduction

[2] Surface accumulation on the East Antarctic ice sheet (EAIS) for periods more than a few decades currently requires ice core information, which is sparsely distributed around the continent. For the purpose of predicting the response of Antarctica to future climate change it is of considerable importance to have an increased knowledge about the past spatial accumulation pattern through time [*Ritz et al.*, 2001; *Parrenin et al.*, 2001; *Ruddiman and Raymo*, 2003; *Parrenin et al.*, 2007]. The aim of this paper is to understand whether and how the spatial pattern of accumulation rate has changed with time over glacial cycles in East Antarctica. Current accumulation-rate maps by *Vaughan et al.* [1999] and *Arthern et al.* [2006], referred to here as AVW, are based on field measurements taken over a period of at most a few decades, as well as instantaneous data retrieved by satellite and, consequently, do not give information about time periods of several hundred thousand years, which have affected the past and present dynamics of the EAIS.

[3] Information about past accumulation rates can be extracted from the positions of isochronous englacial layers, measured by ice penetrating radar, as their geometry is influenced by spatial and temporal changes of past accumulation rates as well as other processes relating to ice flow, such as, for example, flow mechanics and basal melting [*Whillans*, 1976; *Nereson et al.*, 1998, 2000; *Nereson and Raymond*, 2001; *Dahl-Jensen et al.*, 2003; *Fahnestock et al.*, 2001; *Siegert et al.*, 2003, 2004a, 2004b; *Parrenin et al.*, 2006; *Waddington et al.*, 2007; *Eisen*, 2008]. Flow models are needed to predict age-depth relationships and to compare modeled isochrones with those observed. Differences in current and past accumulation rates can then be used in models to infer changes in the flow behavior of the ice sheet. Radar-layer geometry potentially contains much more information than just accumulation. For example, they show how deformation is distributed with respect to depth, which

[1]Physical Sciences Division, British Antarctic Survey, Cambridge, UK.
[2]Department of Geography, Durham University, Durham, UK.
[3]School of GeoSciences, Grant Institute, University of Edinburgh, Edinburgh, Scotland.
[4]Polar Research Institute of China, Shanghai, China.

0148-0227/11/2010JF001785

informs about the significance of sliding, as well as basal melt rate. In principle, these quantities can be inverted for, but the three-dimensional Antarctic problem we are considering is currently too large and complex to be treated in inverse mode. Moreover, such a large and spatially extensive radar-layer data set has never previously been modeled, so that the types of problems that might be encountered are not yet clear.

[4] There have been several previous studies of isochrone architecture in the area we consider: for the South Pole [e.g., *Bingham et al.*, 2007]; for the Vostok region [e.g., *Siegert and Ridley*, 1998; *Bell et al.*, 2002; *Leonard et al.*, 2004] and for the EPICA region [e.g., *Hodgkins et al.*, 2000; *Carter et al.*, 2009]. These focus on smaller horizontal scales than our present study, and in particular are not concerned with large-scale horizontal variations in the flow or recharge of the East Antarctic ice sheet.

[5] We show that a simple 1-D vertical flow model is only able to make useful predictions in certain parts of Antarctica. We then use a three-dimensional numerical ice flow model, which can compute isochrone geometry, to initiate investigation into past accumulation trends from nearly 8000 km of isochronic radar layers, measured from an extensive airborne ice penetrating radar survey of East Antarctica, undertaken during several field seasons in the 1970s. The ultimate aim is to produce a match between computed and observed radar layers while solving for accumulation. The area of the EAIS we consider lies in the quadrant between 90E and 180E. It is a roughly rectangular zone extending from near the pole as far north as Dome C and Vostok. The surface topography and bed topography we use are taken from the BEDMAP compilation [*Lythe et al.*, 2001] with grid resolution of up to 5 km. The layers showing in the radargrams along the radar survey lines are digitally 'picked' from analogue form with a horizontal resolution comparable with the ice thickness. When following the radar survey lines, the resolution is much better than BEDMAP, but the spacing between survey lines is much greater than the 5 km BEDMAP grid resolution. The model is based on the balance velocities approach [e.g., *Budd and Warner*, 1996; *Nereson et al.*, 2000; *Bamber et al.*, 2000; *Le Brocq et al.*, 2006; *Llubes et al.*, 2006] following in particular *Llubes et al.* [2006] in using the inferred modern velocity field to calculate the internal temperature, using the temperature to constrain aspects of the flow field, notably the vertical distribution of velocity (the shape factor) and extending this to a large-scale age calculation. Owing to the computational demands of three-dimensional modeling, we do not use an inverse method as has been done successfully in two dimensions [*Martín et al.*, 2006; *Waddington et al.*, 2007; *Eisen*, 2008]. The paper plan is as follows: in section 2 the approach and objectives are outlined; section 3 discusses the data input, sections 4 and 5 discusses the model and section 6 the model runs. The results are discussed in section 7. When referring to additional information in the auxiliary material, the individual sections, figures, and tables are prefixed with "S."[1]

2. Approach and Objectives

[6] In order to determine a mean spatial pattern of accumulation from the observed isochrone pattern we use a quasi-steady model. In such a model we assume the ice geometry to be steady, and the spatial accumulation-rate *pattern* to be constant. As the absolute accumulation rate can change with time, an equivalent statement to this is that the accumulation rate can be separated into temporal and spatial components. This construction is discussed further by *Parrenin et al.* [2006], who show that while the accumulation rate with a constant spatial pattern affects the age-depth relationship, it does not affect the isochrone geometry. This means that the mean spatial pattern of accumulation rate can be determined. If this is different from the modern pattern, we can conclude that the spatial pattern of accumulation rate has changed with time.

2.1. Quality of Match

[7] Our first goal is to establish the quality of match between observed and modeled radar layers that can be obtained using current spatial accumulation-rate patterns. Our focus is on the regional and continental scales, rather than on more local effects, for example variations in accumulation rate caused by changes in ice-surface slope. If the match is imperfect, we then wish to determine the effectiveness of systematic alteration to the spatial pattern of accumulation rate in improving the match between model and data. In order to do this we need to tease out several rather knotted glaciological issues. A fundamental issue is whether the layer geometry is actually a sensitive indicator of spatial variation in the accumulation rate. This is fairly readily demonstrated by comparing the match with uniform accumulation rate to that obtained with a modern, highly nonuniform spatial accumulation-rate pattern. The next issue is the influence of topography. Where the ice thickness, bedrock, accumulation rate and flow mode are spatially uniform, theory based on continuity predicts flat isochrones, even though the velocity is increasing along a flow line [*Parrenin et al.*, 2006]. Nonuniformity in any of these quantities induces a nonuniformity in the radar-layer geometry. For example, some recent work on the effect of basal topography on isochrone geometry has considered both short-wavelength effects [*Hindmarsh et al.*, 2006] arising from mechanical effects as well as long-range kinematical effects [*Parrenin et al.*, 2006]. Both studies show, in different ways, that nonuniform bedrock topography significantly distorts isochrone geometry. The kinematic effects discussed by *Parrenin et al.* [2006] can, in particular, propagate over very long distances.

2.2. Sources of Errors

[8] A potential for error arises from mismodeling the effect of basal topography on the velocity distribution. In this study we assume shallow ice approximation velocity distributions; however, *Hindmarsh et al.* [2006] show that variations in basal topography over horizontal wavelengths comparable with or shorter than the ice thickness have a strong influence on the velocity distribution. The same problem arises when there are changes in the basal friction over similar wavelengths.

[9] We do not attempt to model these effects, retaining use of the shallow ice approximation in calculating the velocity field. This gives rise to errors in the velocity field which lead to errors in the computed age-depth relationship

[1] Auxiliary materials are available in the HTML. doi:10.1029/2010JF001785.

which in turn cause a mismatch between observed and calculated isochrones.

[10] However, to some extent the mismatch averages out as layers move closer to the bed over crests and further away from the bed in troughs, and the mismatch is essentially local. The main issue raised concerns whether these effects obscure other signals. Since the horizontal scale of these effects occurs when the wavelength of the topography is comparable with the ice thickness, we aim to understand effects with much greater horizontal extent by using the computationally convenient shallow ice approximation. A significant result of the work, discussed in detail in sections 4 and 7, is our quantitative demonstration that we can distinguish between the fit of computed layer geometries from different accumulation-rate scenarios to observations, despite the occluding effects of the topographic mismatch.

[11] Where radar survey lines cross flow lines, an immediate issue is whether our ignorance of the bed along flow lines impacts, or even eliminates, the possibility of obtaining a match between observed and computed radar-layer elevations. One way of investigating this is by comparing the solution using grids with a different cell size. Provided these grids are above or at the resolution of the grid used to generate the topography, this amounts to a sensitivity study on the required level of detail of topography. This mismodeling from data ignorance occurs whatever the wavelength, and here we have to consider the possibility of long distance propagation of effects as outlined by *Parrenin et al.* [2006]. Such investigations are reported in this paper in section S6 of the auxiliary material.

2.3. Changes in Flow Mode

[12] Other unresolved influences, for example spatial changes in the flow mode from internal deformation to sliding, might be expected to contaminate the match for similar reasons. *Hindmarsh et al.* [2006] and *Parrenin and Hindmarsh* [2007] consider short and long-wavelength consequences of changes in flow mode respectively, while the latter paper also addresses the effects of basal melting. Some of the possible complications in three dimensions arising from these kinematical effects are shown by *Leysinger Vieli et al.* [2007]. Again there are possibilities of short-wavelength and long-wavelength effects. Changes in flow mode can arise from thermomechanical effects, and other thermally induced processes such as basal melting are likely to contaminate the match. The overall effect of these on the match are investigated in this paper through sensitivity studies involving changes in the flow mode.

[13] To assess these issues of changes in flow mode, we run the full three-dimensional model, which incorporates horizontal advection, and permits nonuniformity in the vertical profile of the velocity (i.e., can relax the plug flow assumption). We can also compute basal melt on the basis of the assumed geothermal heat flux. Geothermal heat flux in Antarctica has a significant effect on the age at the base of the ice sheet [*Huybrechts et al.*, 2007; *Ritz et al.*, 2001; *Llubes et al.*, 2006; *Pattyn*, 2010] and is poorly known [*Shapiro and Ritzwoller*, 2004; *Fox Maule et al.*, 2005]. Our approach in this paper is not to attempt to represent the geothermal heat flux exactly, but to investigate its effect on isochrone geometry, as shown in section S6 of the auxiliary material.

2.4. Spatial Changes in Accumulation Rate

[14] It is clear even from the radargrams that some isochrones dip over long distances, which is suggestive of spatial variation in accumulation rate. It is also known that the smaller scale pattern changed with time, for example, the presence or absence of blue ice [*Siegert et al.*, 2003], but the main result of this paper is that we can infer from the radar-layer data that the large-scale spatial pattern of accumulation rate changed with time (over tens of thousands of years). This is in addition to the well known result from ice cores that the absolute value changed over time. The accumulation rate was roughly half during glacial periods [see *Lemieux-Dudon et al.*, 2010, Figure 9]. We can make this inference because we can obtain a better match to the layers using a different spatial accumulation-rate pattern to the present-day one, but to completely convince, we show that the confounding factors mentioned above, topography, computational grid size, flow mode and geothermal heat flux, while contaminating the match, do not do this to the extent of obscuring the long-range accumulation-rate signal.

3. Data and Model Input

[15] We use airborne radar data (60 MHz, 250 ns pulse length) sampled during the 1970s by the Scott Polar Research Institute (SPRI), the US National Science Foundation (NSF) and the Technical University of Denmark (TUD) [e.g., *Neal*, 1976; *Robin et al.*, 1977; *Drewry and Meldrum*, 1978; *Turchetti et al.*, 2008]. The line coverage is shown in Figure 1. These data, originally in analogue form, have been scanned to digitally pick the layers. Digitized layers are matched to position using a time marker on the records, linked to latitude and longitude. Internal layers are believed to be isochronous [*Fujita et al.*, 1999; *Hempel et al.*, 2000], representing paleo-ice surfaces that have been buried and advected by ice movement. Strongly reflecting internal layers, recorded by the ice penetrating radar, are picked along the radargram and, where possible, matched at crossovers with layers from other radar survey lines. The digitized, geolocated internal layers are able to be used as an input to the numerical model. Table 1 presents statistics about each radargram picked, revealing the length of the radar survey lines, the number of layers picked, the number used and the mean sampling step. Other model inputs include the modern surface geometry of Antarctica and the bed geometry from BEDMAP [*Lythe et al.*, 2001] and the spatial surface accumulation-rate pattern AVW [*Arthern et al.*, 2006], which are needed to calculate the modern balance fluxes and the depth age field.

[16] The vertical accuracy has been maintained and assured by (1) picking many layers showing in a radargram and by using several crossovers of survey lines to connect the data; (2) reducing the layers for model input to only the best layers, showing distinctive and extended reflections; and (3) using several crossovers to reduce the errors from assuming that the picked layers are the same over a cluster of radar lines. For each radargram we tried to pick as many reflecting layers as possible (Table 1) to ensure that the errors from skipping from layer to adjacent layer were kept small [*Leysinger Vieli et al.*, 2004]. Subsequently the layers were pruned (see below) and digitally picked. More detailed information can be found in the auxiliary material. An

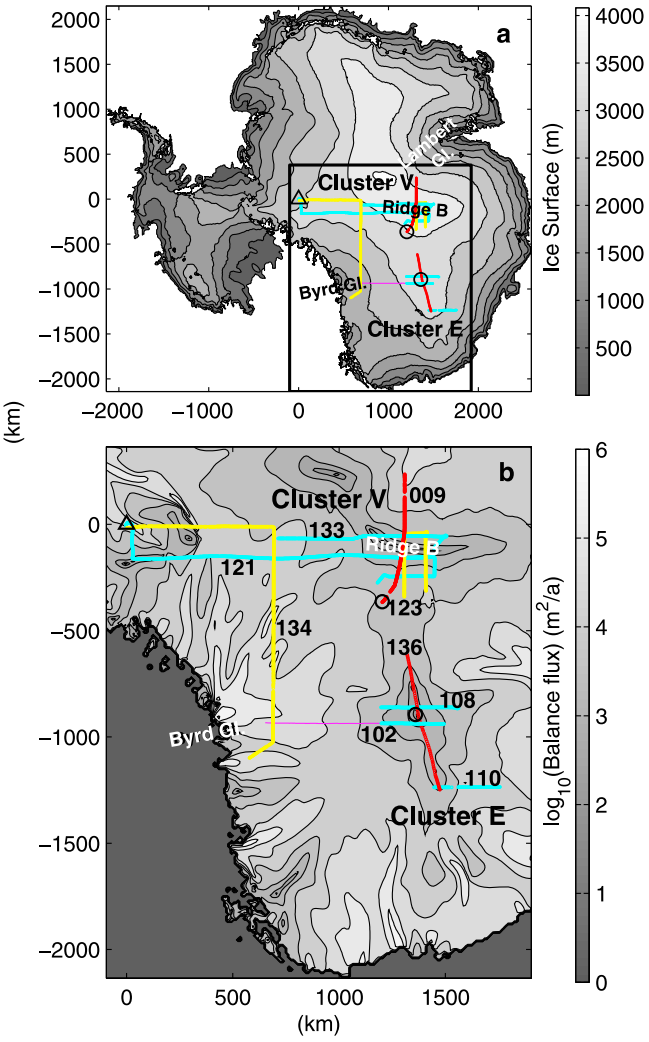

Figure 1. Map of Antarctica with radar survey lines used in the models and names of localities used in the text. (a) Ice surface (contour interval, 500 m). Circles denote position of ice cores (EPICA and Vostok), and the triangle locates the South Pole. (b) Balance velocities (contour interval, 0.5 $\log_{10}$ (balance flux) $m^2\ a^{-1}$) with the radar survey lines labeled for a section of East Antarctica. Clusters are connected to an ice core by a radar survey line (red) either going through or passing close by (detailed information about colored radar survey lines is found in section S2 of the auxiliary material). Clusters E and V are in the vicinity of EPICA Dome C and Vostok, respectively. The age-depth relationship of the radar survey lines for each cluster can be obtained from their respective ice cores (circles). See text for stratigraphic correlation of these clusters.

introduction to the auxiliary material is given in section S1, information on data coverage is given in section S2, while further discussion of data processing procedures, and sources of error, can be found in section S3. The picked topography and the BEDMAP topography did not coincide exactly, the implications of which are discussed in section S4.

[17] We have generated two clusters of correlated layers. In the first cluster we were able to connect 4 radar survey lines (136, 108, 102, 110) by correlating 5 layers within those survey lines (hereafter Cluster E, numbered 3, 5, 9, 11, 12) and in a second cluster to connect 5 radar survey lines (009, 121, 123, 133, 134) by correlating 7 layers within (hereafter Cluster V, numbered 1, 2, 4, 6, 7, 8, 10). The Cluster E is situated around EPICA Dome C and Cluster V between Lake Vostok and Ridge B, and runs toward South Pole. The 5 layers used in Cluster E range from 32,000 years to 300,000 years and the 7 layers from Cluster V from 30,000 years to 180,000 years. The ages are those calculated respectively by *Parrenin et al.* [2007] (EPICA) and *Ruddiman and Raymo* [2003] (Vostok). The layers do not go through EPICA exactly, so to find their age at the point on the radar survey line 136 nearest to Dome C (at a distance of 13 km), we used the same age-depth relationship based on the normalized depth as obtained from the EPICA ice core. For further information on data coverage see section S2 in the auxiliary material.

[18] Figure 2 shows a fence diagram of all the picked layers correlated with age-depth relationship from the Vostok (Cluster V) or EPICA (Cluster E) ice cores. We call this setup the Separated Cluster case (SC case), which consists of 12 layers. It might appear from Figure 1 that we should be able to correlate the two clusters using radar survey line 102, but unfortunately there is an area within survey line 102 where the reflection of the layers are very weak and hard to see. Consequently, we adopted the procedure of correlating the layers using the ages from the ice core and assumed that layers in the Vostok core were identifiable with layers in the EPICA core. We call this the Combined Cluster case (CC case), which has three layers which are assumed to be the same in both clusters. The correlated layers are (2,3), (5,6) and (8,9) (Figure 2). More on correlating the data can be found in section S3 in the auxiliary material.

[19] Preliminary experiments showed that the quality of the fit (how well the picked and modeled layers match) was affected by the vertical spacing of the layers. If too many layers too close together were used, this resulted in the fit being good at the elevations of these closely spaced layers, but could result in quite poor fits at other (usually deeper) layers. Pruning the data to ensure an even spacing of lines ensured a much more vertically uniform quality of fit (see also section S3). This problem has been addressed by *Nereson et al.* [2000] who used a weighting based on spacing, but, given the high correlation between closely spaced lines we felt that pruning (removal of the line with the worst data quality, such as vertical uncertainty due to the many gaps and forks in the data) was as effective, especially in view of the fact that the picking process introduces correlations between closely adjacent layers.

[20] Figure 3 shows the input data to the model at the resolution used in the model, the spatial accumulation-rate pattern AVW, the ice-surface topography and ice thickness [*Lythe et al.*, 2001], and the computed balance velocities. The surface topography includes sinks, the presence of which contradict some assumptions used in the computation of the balance velocities. The sinks are removed by smoothing the surface slopes, which affects (smooths) the velocity direction, but unsmoothed thicknesses are used to compute the balance velocity from the balance flux. The

Table 1. Radar Survey Line and Picking Information

Radar Survey Line	Length	Horizontal Sampling Step	Number of Picked Layers	Number of Used Layers
		Cluster Dome C		
136[a]	654 km	8.48 km	25	4
108	366 km	2.44 km	26	4
102	295 km	2.52 km	18	5
110	311 km	3.2 km	19	2
		Cluster Vostok		
009[b]	629 km	2.02 km	25	7
133	885 km	2.51 km	16	3
121	2000 km	2.35/0.89 km	21	6
123	700 km	2.67 km	15	3
134	1842 km	3.02 km	19	3

[a]Radar survey line located approximately 13 km from Dome C borehole.
[b]Radar survey line going through Vostok borehole.

balance velocities exhibit similar complex streaming patterns to those discussed by *Bamber et al.* [2000].

4. Preliminary One-Dimensional Analysis

[21] Before launching into discussion of a full three-dimensional model, it is worth examining whether a simpler, one-dimensional model that focuses on vertical flow only is sufficient to analyze the radar layers. Figure 4a shows the aggregated layers for the CC case, surface and bed plotted line by line, while Figure 4b shows the normalized elevation of each layer. Under steady state, where plug flow occurs and horizontal advection can be ignored, the age X is given by the Nye age-depth relationship [*Nye*, 1963]

$$X = \frac{H}{a}\ln(\zeta), \tag{1}$$

where H is the ice thickness, a is the accumulation rate, $\zeta = (z - b)/H$ is the normalized elevation; here z is elevation within the ice and b is the elevation of the bed. Figure 4c

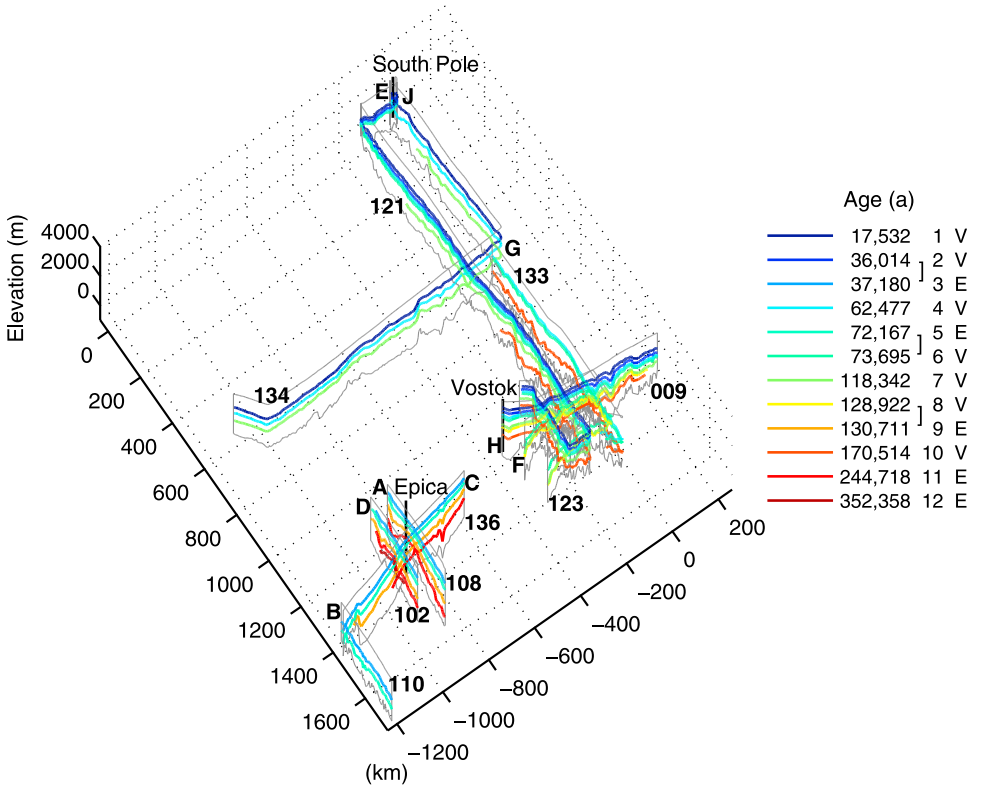

Figure 2. Fence diagram of radar survey lines showing picked surface and bed (both in gray) and picked layers, color-coded according to age for the SC case. Ages are deduced from Vostok and EPICA ice core. The legend shows three columns for each layer: the age, the layer number as used in the text for the SC case, and the cluster to which it belongs. The square brackets in the legend show joined layers for the CC case. Note that the capital letters mark the start (0 km) of the respective radar survey line.

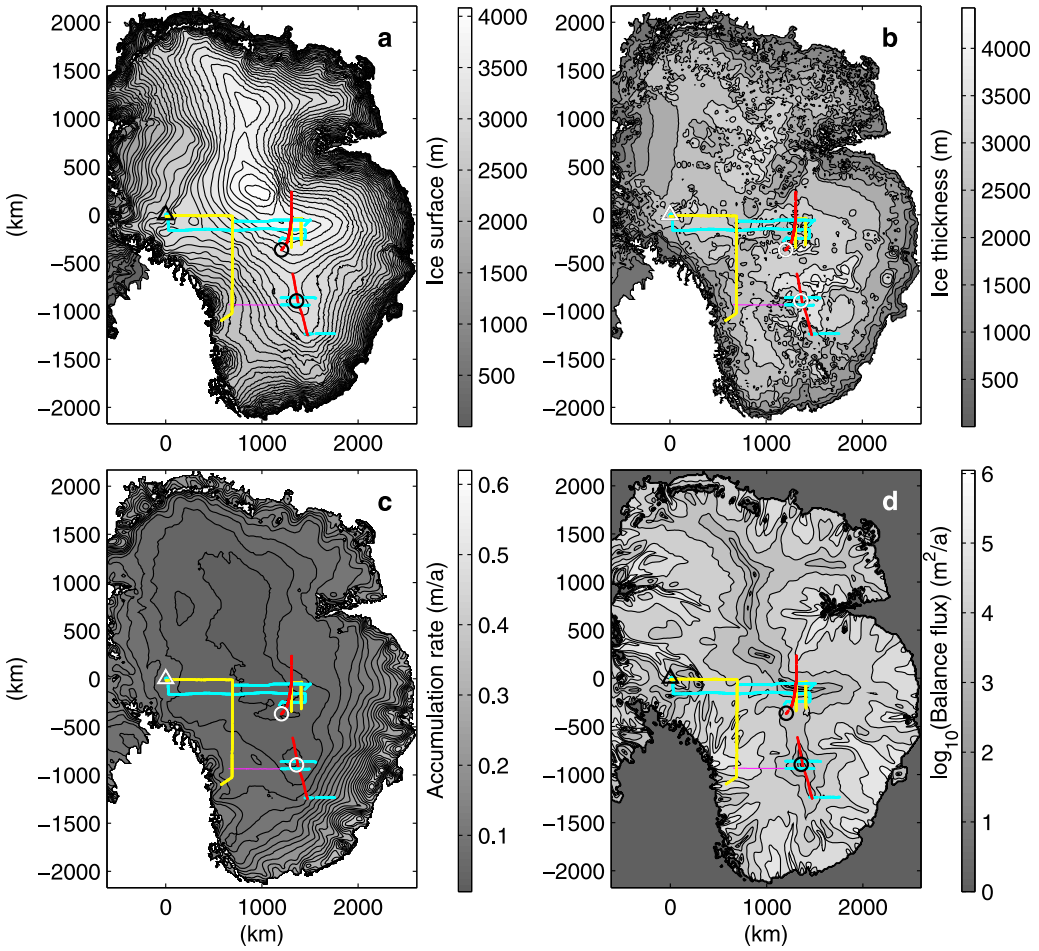

Figure 3. Input data for three-dimensional numerical model: (a) ice surface [*Lythe et al.*, 2001], (b) ice thickness [*Lythe et al.*, 2001], (c) spatial accumulation-rate pattern AVW [from *Arthern et al.*, 2006], and (d) computed balance (column-averaged) velocities on the grid used. Radar survey line color-coded as described in Figure 1. Contour intervals for subplots are 100 m, 500 m, 0.02 m a^{-1}, and 0.5 $\log_{10}$ (balance flux) m^2 a^{-1} for Figures 3a–3d, respectively.

shows the time-averaged accumulation rate inferred from the topmost layer using equation (1) and spanning a period from 17.5 ka to present, as well as the modern accumulation rate from AVW. It is clear that the patterns are very similar, although there is a slight but systematic difference in the rate. In fact, a can be treated more generally as the mean accumulation over the period from the age at the depth of interest up to now.

[22] By a fairly simple analysis of the layer data, we can determine whether the assumptions used to generate equation (1) hold. Firstly, if the assumptions of plug flow and low horizontal advection hold, then it is also true that even under nonsteady conditions the difference in age between two isochrones ΔX is proportional to $\Delta\ln\zeta$ at any given horizontal point, with the coefficient of proportionality α also equal to H/a. This is essentially a null hypothesis, so we call this Model H0. Note that H/a is a function of position, and in consequence we expect α to vary in space.

[23] We now consider this ratio $\alpha = \Delta X/\Delta\ln\zeta$, for each isochrone pair, plotted along a given radar survey line, or a section of the survey line, wherever there are several (more than two) isochrones. Then, if the plug flow/low horizontal advection assumptions are locally valid and the spatial pattern has remained constant in time, the ratio $\Delta X/\Delta\ln\zeta$ for each of the layer pairs will have the same pattern as a function of position. Furthermore, where these assumptions hold, we may find an optimal scaling parameter for each of these $\Delta X/\Delta\ln\zeta$ such that they all plot exactly on top of one another for those radar survey lines sections where the assumptions are true. This is further explained and illustrated in section S7 in the auxiliary material.

[24] In Figure 5a we plot $\alpha = \Delta X/\Delta\ln\zeta$, normalized by the transect mean, against point number for the whole data set. The transects correspond to the radar survey lines, except that survey line 121 has been split into two parts, called 121a and 121b, as this allowed improvement in the overlay in the two parts. It can be seen in some parts of the plot (transects 121a, parts of 121b, 123 and 133 in the Vostok cluster, and transect 108 in the EPICA cluster) that the normalized α plot over one another. In other transects (009, 134) in the Vostok Sector, (110, 136, 102) in the EPICA sector, the approach is unsuccessful, as is the case in the other part of transect 121b. Where the approach is successful, we can say that the assumptions of (near-)plug flow,

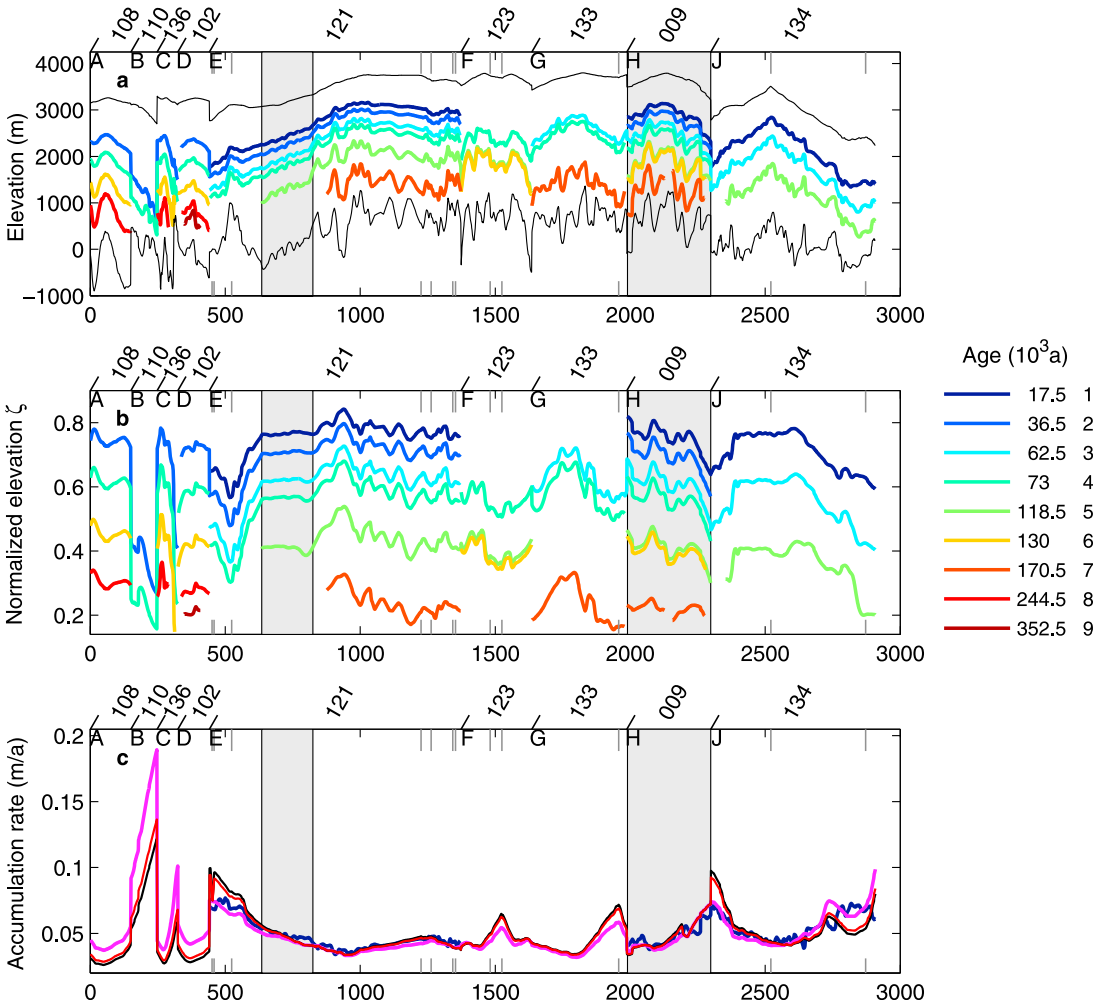

Figure 4. (a and b) Picked layers and (c) accumulation rates of all radar survey lines (labeled). Figure 4a shows picked surface, bed (black), and layer elevation for each sampling point. Figure 4b shows layer elevation normalized by ice thickness. Legend shows rounded layer ages and layer numbers for the CC case (numbers 2, 4, and 6 represent layers 2/3, 5/6, and 8/9 in Figure 2, respectively). Figure 4c shows accumulation rate inferred from the topmost layer (blue), modern accumulation rate (magenta) from AVW, and tuned accumulation rate (thin line) for the SC (black) and CC (red) cases. Note that the radar survey line number, its extent (inclined ticks), and start (capital letter) are shown at the top. Gray ticks mark position of sharp bend in survey line. Gray shaded boxes highlight the same area as Figure 5.

low horizontal advection and constant spatial pattern of accumulation rate are valid.

[25] The simple model of ice flow represented by equation (1) is consequently not applicable to the whole of East Antarctica, implying that the set of assumptions lying behind equation (1) are somehow in error. The removal of some of these simplifying assumptions requires a more sophisticated three-dimensional flow model. We could have diagnosed this more precisely using the approach of *Waddington et al.* [2007, section 6.5], who give quantitative criteria for determining whether accumulation or thickness gradients have affected isochrone geometry.

5. The Three-Dimensional Quasi-Steady Model

[26] The model we use is described fully by *Hindmarsh et al.* [2009]. The model is quasi-steady; that is, we assume the ice geometry to be steady, and the accumulation-rate *pattern* as a function of horizontal position to be constant. The absolute rate of accumulation can change with time. This construction is discussed further by *Parrenin et al.* [2006]. In other words, with the modeling procedure we use, we can investigate the assumption that the accumulation rate can be described as the product of temporal and spatial components. In addition, the modeling allows us to determine the mean spatial pattern of accumulation, at least over the depth and corresponding time where layers are present. If this is different from the modern pattern, we can conclude that the spatial pattern of accumulation rate has changed with time.

[27] The method consists of the following.

[28] 1. Compute the balance velocities using the tensor grid method of *Hindmarsh* [1997].

[29] 2. Choose shape functions to describe the velocity. This might include plug flow (horizontal velocity independent of depth) or functions which represent the way

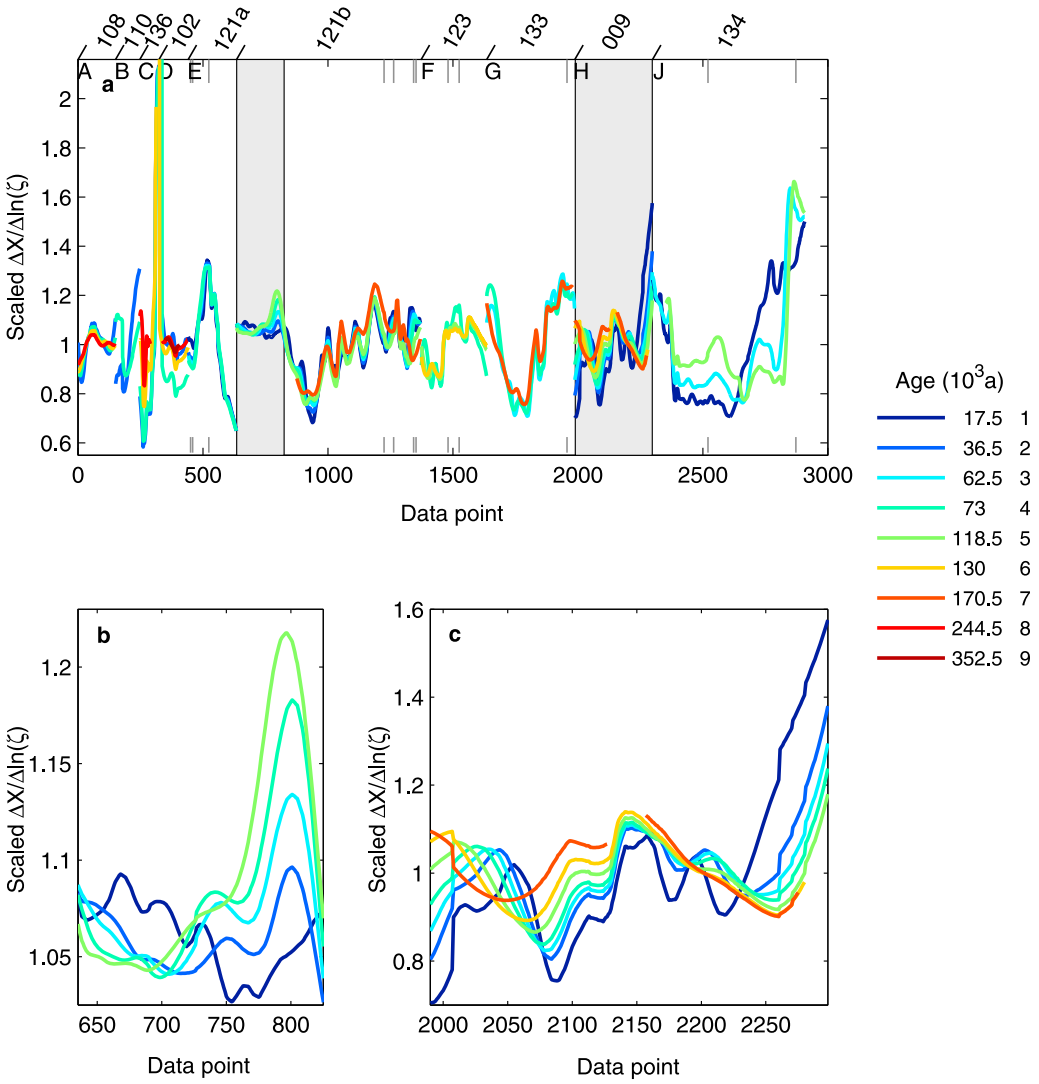

Figure 5. Assessing validity of one-dimensional flow assumptions. (a) The quantity $\alpha = \Delta X/\Delta \ln \zeta$ scaled by its mean value for different survey lines plotted for each layer pair (surface used as first layer). Layer pair color code is using color of the older layer. (b and c) Blow-ups of highlighted areas in Figure 5a where the values of α do not overlie each other. See also section S7 and Figure S6 in the auxiliary material for more details on Model H0. Legend and labeling as in Figure 4.

shearing varies with depth as predicted by the shallow ice approximation.

[30] 3. Apply these shape functions in ice and heat transport equations and generate and solve finite difference approximations to these equations [*Hindmarsh et al.*, 2009]. The governing equations can describe the motion of tracers, age contours or heat.

[31] 4. Where temperatures are solved and used to determine or compute the shape function, we move back to step 2 and iterate until a consistent set of shape functions are obtained. We term this a "thermally coupled" case.

[32] 5. The age solution is computed.

[33] 6. Computed age contours (modeled isochrones) are compared with data (internal layers).

[34] The method requires upper-surface and basal topography, accumulation rate, prescribed rate of change of thickness (zero everywhere in these studies), shape functions, and either a prescribed geothermal heat flux (if temperature calculations are performed) or prescribed basal melt rate.

[35] In this study we use two types of shape functions υ for the horizontal velocity (uniform plug flow (equation (2a)) and internal deformation (equation (2b))),

$$\upsilon(\zeta, \mathbf{r}) = 1 \tag{2a}$$

$$\upsilon(\zeta, \mathbf{r}) = \frac{(n+2)}{(n+1)}\left(1 - (1-\zeta)^{n+1}\right), \tag{2b}$$

which derive from the shallow ice approximation, where n is the Glen index, set to 3 in this study. Basal warming without sliding causes the flow to become more plug-like. In areas

Table 2. Summary of Model Runs Carried Out

Calculation Series	Variables	Influence
Accumulation distribution	accumulation pattern	significant
Flow mode	plug flow or internal deformation	slight
Geothermal heat flux	40, 45, 50, 55, and 60 mW/m_2	extremely slight
Horizontal advection	on or off	significant
Grid size	5, 10 and 20 km	slight

where the topography has a wavelength comparable with the ice thickness, these shape functions do not apply, especially near the base.

[36] The solution procedure is to start off with a zero melt rate and a velocity distribution corresponding to isothermal internal deformation. On the basal boundary the flux is set to equal the geothermal heat flux plus the dissipative heat flux. By including the dissipative heat flux here rather than distributing it through the column, we are using the plug flow approximation of *Fowler* [1992], which also gives a formula for computing the corresponding heat flux at the base of the ice. Solutions of the equations produce a temperature field, and in general some points will have a computed temperature above the melting point. Where this occurs, the basal boundary condition is reset to a prescribed temperature (pressure melting point), and the temperature field recomputed. Where the temperature is prescribed on the boundary, the melting rate is computed and the effect of this on the vertical velocity field accounted for. This same procedure is repeated until there is no change in the temperature field. In each case, a slightly different velocity field is obtained, and the effect of this on the match to the observed isochrone geometry is computed.

[37] Once the age field is computed the computed isochrone that best fits a given observed layer is found by minimizing the sum of the squares of the misfit, the difference in elevation measured in normalized coordinates [*Hindmarsh et al.*, 2009]. Using normalized coordinates stops the procedure weighting in favor of areas where the ice is thicker.

6. Model Runs

[38] A large number of calculations were carried out varying the spatial accumulation-rate pattern, the flow mode, the geothermal heat flux, the grid size, and the consideration of horizontal advection. The calculations are summarized in Table 2. The aim of the calculations was to determine whether the breakdown of the plug flow/no horizontal advection model (Model H0) is due to failures in the glaciological assumptions or the climatological assumptions.

[39] We summarize the calculation series as follows, presenting the detailed results in the next sections.

[40] 1. We compared the match obtained for three accumulation-rate maps AVW, *Vaughan et al.* [1999] and uniform spatial accumulation rate to determine which of the these spatial patterns produced the best fit.

[41] 2. Using the best fitting spatial accumulation-rate pattern (AVW), our next concern was whether the variability in flow mode (plug flow or internal deformation) had a significant influence on the match. In order to simulate the horizontal distribution of sliding and internal deformation, we computed basal temperatures using different assumed geothermal heat fluxes and also different assumptions about the flow mode. We also derived basal melt rates, which affect vertical velocity and can affect isochrone shape at depth. We found that these sensitivity studies regarding the flow mode and geothermal heat flux influenced the match only slightly, which is further discussed in section S6 of the auxiliary material.

[42] 3. A similar concern about grid resolution of the computational (i.e., BEDMAP) grid caused us to compare results computed on a 20 km, 10 km and 5 km grid. In all these cases, we saw a strong and consistent long-range pattern, which we concluded was due to misspecification of the time-averaged accumulation rate (see section S6 for results on sensitivity study).

[43] 4. Finally, we adjusted the accumulation rate in order to improve the match using models with uniform flow mode. Our concern was to obtain some quantitative indications in the long-scale variation of the accumulation rate required to match the radar-layer geometry, to see if time dependence was significant, and to see if signals from ice-dynamical variability could be seen. Some further calculations also investigated whether excluding horizontal advection, which is appropriate for divide areas, significantly altered our conclusions. Note that as a shorthand for no horizontal advection and including horizontal advection we use 'HA off' and 'HA on,' respectively.

[44] Using the AVW spatial accumulation-rate pattern, we briefly discuss the basal temperature patterns in order to show that we considered an extensive range of scenarios, which most likely encompass the true situation in order to strengthen our understanding that the temperature pattern/flow mode does not affect the quality of the match of model and data.

[45] Figure 6 shows basal temperature patterns, as a function of three geothermal heat fluxes, and selected dynamics options. These show, in common with other studies based on different configurations, that the very poorly known geothermal heat flux has a major control on the distribution of melting [*Huybrechts et al.*, 2007; *Ritz et al.*, 2001; *Llubes et al.*, 2006; *Pattyn*, 2010]. Some subtle differences are observed between the no horizontal advection option (slightly warmer), the plug flow option (generally cooler) and the self-consistent thermally coupled shape function option. Including horizontal advection allows the cooler ice from higher central areas to be advected in; plug flow allows higher vertical velocities near the bed, which allow colder ice to penetrate nearer the bed and thus cool the bed.

[46] Figure 7 shows basal melt rate. Basal melt rate is potentially important in East Antarctica, where accumulation rates can be very low so as to be only slightly greater than basal melt rates (see Figures 3 and 7). In such places, the basal melt rate can have a substantial effect on the vertical velocity and, consequently, isochrone geometry.

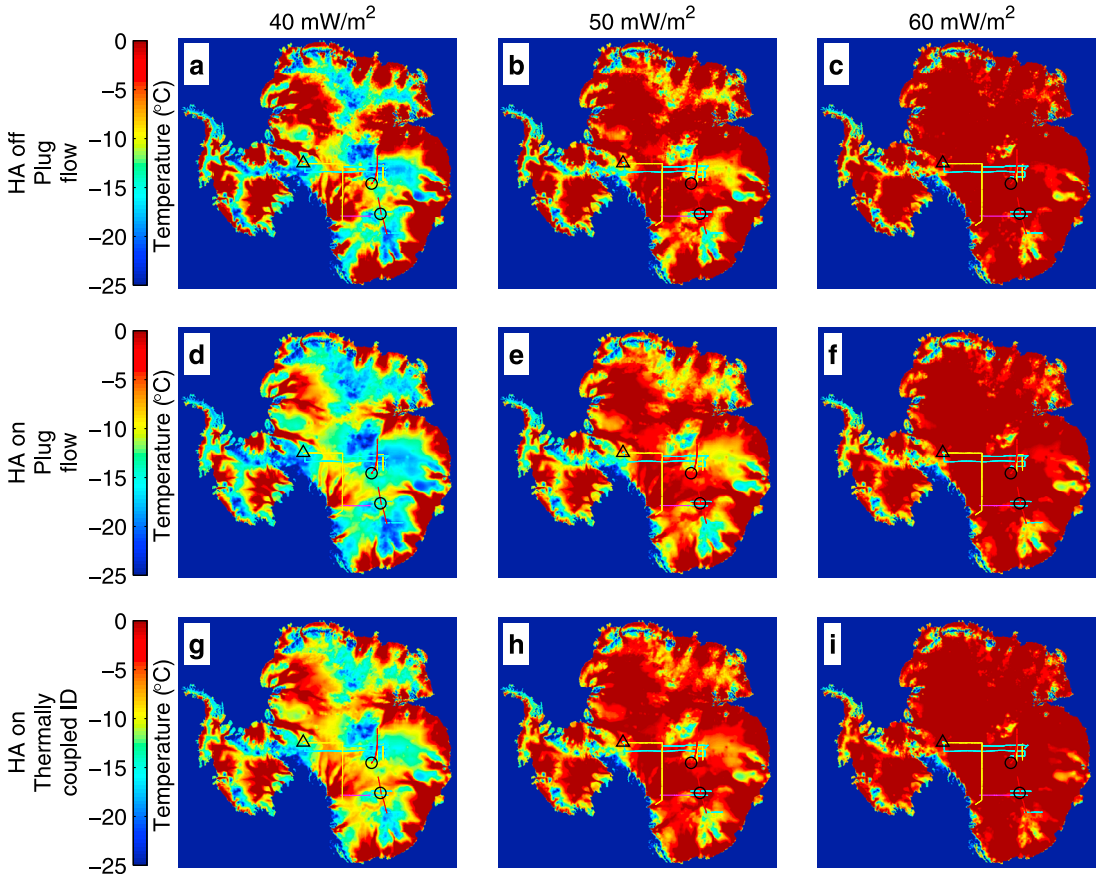

Figure 6. Computed steady basal temperature field as a function of indicated geothermal heat flux. Calculations used balance velocity field and dissipation; (a–f) the first two rows are plug flow, and (g–i) the bottom row has internal deformation with thermally adjusted shape functions. Figures 6a–6c have no horizontal advection. The radar survey lines are overlying the images (see Figure 1 for description).

Figures 7a–7i show that high melt rates are strongly associated with high velocities toward the ice sheet margin. These areas do not generally correspond to the areas where our radargrams were obtained, however.

7. Results

[47] We now consider the mean square misfit, reported as the mean of the square misfit measured in units of normalized thickness. The mean square is summed pointwise rather than weighted by distance; this means that higher weighting is given to areas where the radargram was sampled more frequently, generally where its isochrone geometry was more variable. We also tried weighting the fit by the horizontal distance between points. We found that the difference between calculating the mean square misfit with and without weighting was not substantial.

[48] Mean square misfits are reported in Table 3 and in Tables S1 to S6 in the auxiliary material. Tables S1 and S2 show the results for CC and SC case, respectively. The results from the different calculation series detailed in the tables mentioned above and summarized in Table 2 show that including horizontal advection (HA on) decreases the mean square misfit substantially, that having a varying flow mode decreases the mean square misfit slightly, and that at least a spatially uniform geothermal heat flux is not a significant factor. Results are distinctly better when the clusters are not combined (SC case). The reason for this is that for the CC case there are more constraints upon the layers than for the SC case. The total fit for all combined layers must be worse, but this does not exclude that individual layers of the CC case show a better fit than the same layers for the SC case. Tables S3 to S6 look at the distribution of mean square misfits between clusters and layers in more detail, showing that mean square misfits are not redistributed between clusters and layers as the parameters are changed. More information on the mean square misfit for clusters and layers can be found in the auxiliary material section S8.

7.1. Spatial Patterns of Misfit With the AVW Accumulation-Rate Map

[49] We consider some of the spatial aspects of the misfit. Here we state the misfit in terms of normalized ice thickness, and note the sign of the misfit as well. We define it in terms of the computed elevation above the bed (normalized by the ice thickness) minus the observed elevation, so a positive misfit means the computed layer is above the observed layer. Figure 8 shows fence diagrams of the misfit for AVW, SC (Figure 8a) and CC (Figure 8b) cases. We do

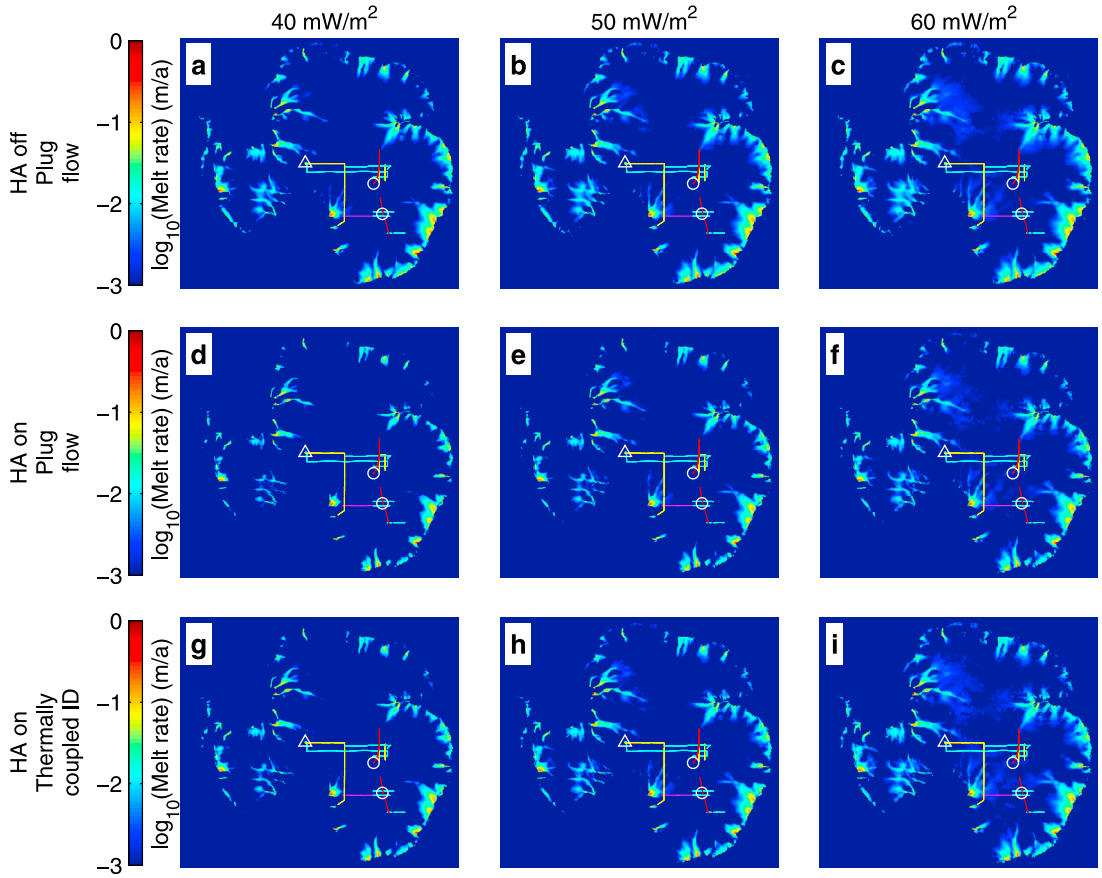

Figure 7. Computed steady basal melt rate as a function of indicated geothermal heat flux. Cases as for Figure 6. The radar survey lines are overlying the images (see Figure 1 for description).

not attempt to reconcile these with the more localized studies of the area cited in the introductory section [*Siegert and Ridley*, 1998; *Hodgkins et al.*, 2000; *Bell et al.*, 2002; *Leonard et al.*, 2004; *Bingham et al.*, 2007; *Carter et al.*, 2009], as we are focusing on much larger spatial patterns.

[50] The spatial patterns in the misfits for the SC and CC cases are similar, although the absolute misfit in the CC case is greater. Near the South Pole, there is a mostly positive misfit. Along the lines from the South Pole to Vostok, the misfit alternates between positive and negative with range of around +0.15 to −0.1, with a horizontal spatial scale of around 400–500 km along 121 and the parallel parts of 134 and 133. Around Vostok the misfit is −0.15, while northwest of Vostok the misfit is positive, with a maximum of 0.1. On the Lambert Glacier (western) side of Ridge B, the misfit is slightly positive. From the middle to the far end of line 134 running subparallel with the Transantarctic Mountains, the misfit is negative, varying between 0.0 and −0.2 over length scales of 200–400 km. In the EPICA cluster, in the central part of Line 136, the patterns of the SC and CC cases are similar; the SC case has more positive misfits compared with the CC case. There are stronger short-scale (100 km) trends in the EPICA cluster compared with the Vostok cluster at the ends of Line 102, 108 and 136. The one exception to this correspondence in the spatial pattern is in the northern part of the EPICA cluster, where misfits are of opposite sign on parts of 110 and 136 near where they join.

[51] A general outcome of the matching process was that the layer length correlates inversely with the quality of the fit. The cause of this is fairly obvious; it is not the elevation of a layer which requires explanation by ice flow modeling, but the variability of normalized elevation with horizontal position. In general, along a short section the flow field, which impacts on the layer elevation, the misfit is more uniform than along an extended section. Therefore the layer

Table 3. Showing Influence of Accumulation Distribution on Mean Square Misfit[a]

Accumulation Distribution	Misfit, SC case (12 layers)	Misfit, CC case (9 layers)
Uniform	6.62	6.68
Arthern and others (2006)	3.05	3.64
CC case fit	2.30	**2.36**
SC case fit	**2.24**	2.58

[a]Misfit $\times 10^{-3}$. Bold numbers highlight best fitting spatial accumulation-rate patterns for each case.

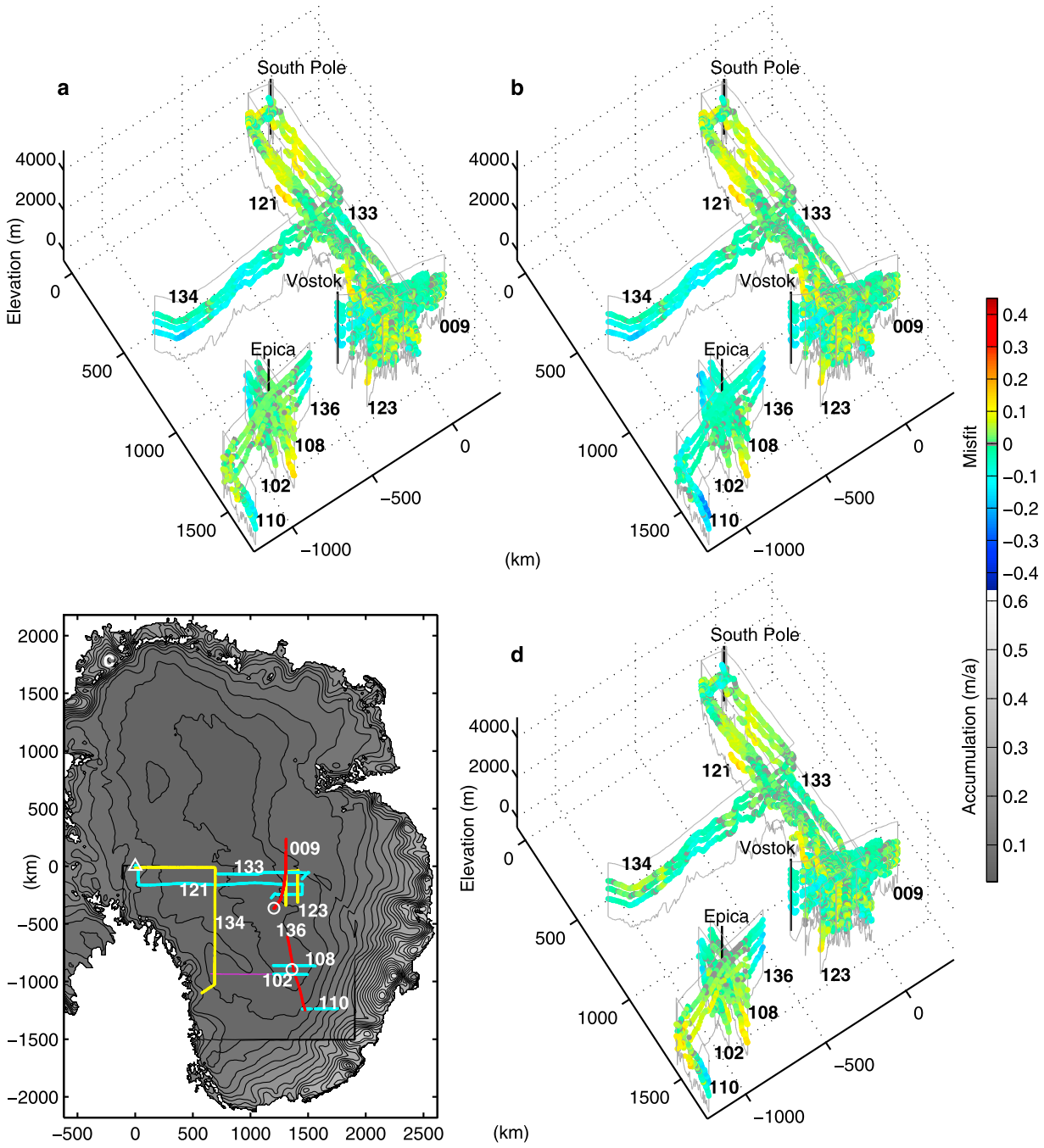

Figure 8. Illustrating the misfit. Fence diagrams of the misfit for modern (AVW) accumulations for (a) SC and (b) CC cases. (c) Map of tuned accumulation for the CC case (accumulation pattern can be compared with Figure 3c; contour interval at 0.02 m a^{-1}). (d) Fence diagram of the misfit for the CC case, with the tuned accumulation fit. Calculations used 10 km grid, plug flow, and geothermal heat flux of 50 mW/m^2. Note that zero misfit is shown by gray dots. See also Figure 2.

geometry of short sections is expected to be more readily 'explainable' in the sense that the controlling parameters are less likely to require spatial tuning.

[52] Figure 9a shows a plan view of the misfit between model and data for the connecting layer with the lowest overall misfit for a geothermal heat flux of 50 mW/m^2, spatially varying velocity shape functions, for the CC case. We see that the misfit is generally ±0.1 normalized thicknesses. Within the radar survey lines comprising the clusters there is variability in the misfit, and some examples are shown in Figures 9b–9d, ranging from the best case (Figure 9b, line 009), showing smallest deviation of the misfit from zero, to an intermediate case (Figure 9c, line 102) to the worst case (Figure 9d, line 110), where we find a maximum negative

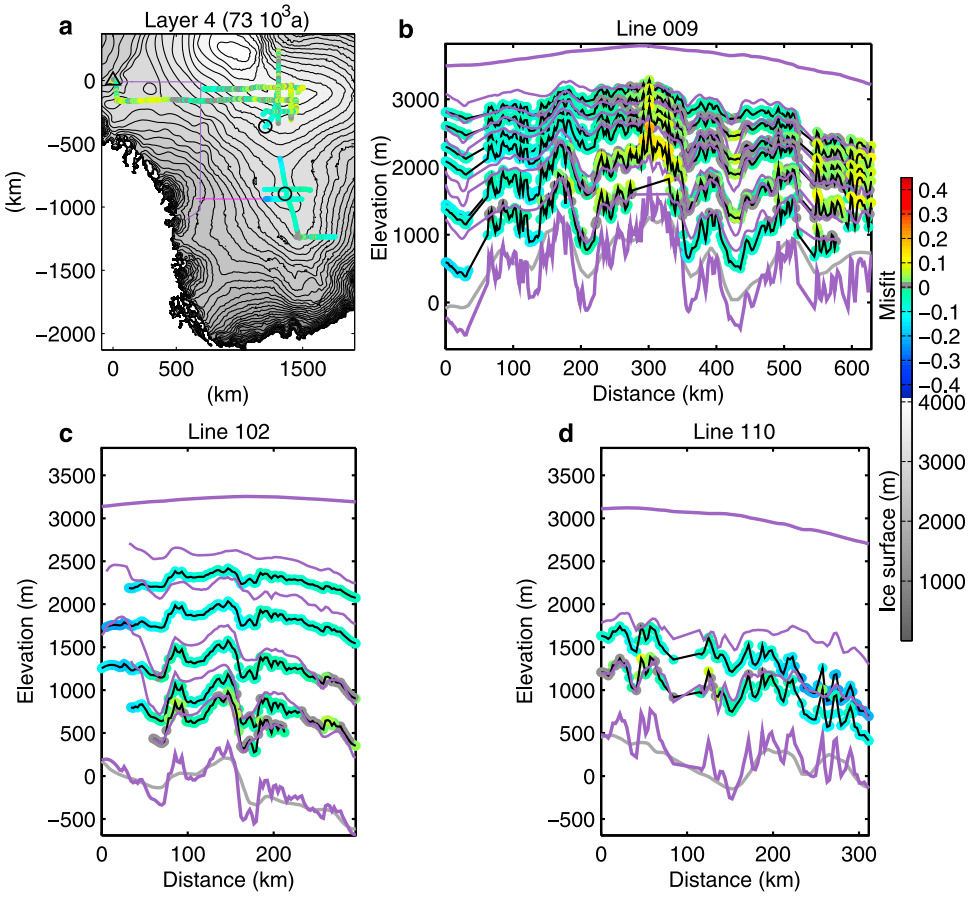

Figure 9. Illustrations of fit and misfit for the CC case. (a) Misfit of layer of CC case with highest goodness of fit along radar survey lines (purple); ice surface contour interval at 100 m. (b–d) Radar survey lines show misfit for cases with low misfit (Figure 9b) and increasing misfit through Figures 9c and 9d. Observed (picked) layers are purple, modeled layers are black with color coding for the misfit, gray is the BEDMAP bed, and purple bed is the picked bed. Positive misfit means that the modeled layers are above the picked ones; zero misfit is shown by gray dots. Calculation was thermally coupled (geothermal heat flux of 50 mW/m^2) using spatially varying velocity shape functions (thermally coupled ID), age distribution as for the CC case, and AVW spatial accumulation-rate pattern with horizontal advection (HA on). Note that the result is plotted in the picked data grid (see also section S4 in the auxiliary material).

misfit of almost −0.2 normalized thicknesses. Line 009 has a very good overall fit apart from the left end which corresponds to Lake Vostok, where the model assumptions break down anyhow. In the other cases it is not evident why the model should not work apart from invoking the explanation of incorrectly specified temporally averaged accumulation rate. In particular the rise in the observed layers above the computed layers, seen toward the left in line 102, are rather hard to explain and might be related to quite severe relief in the area. More detailed plots of the misfit on a layer-by-layer basis are shown in section S5 of the auxiliary material, while the influence of the geothermal heat flux, the grid size and the influence of horizontal advection are considered in section S6.

[53] Figure 10 shows plots of the misfit envelope for a chaining of the radar survey lines, for a number of different scenarios. The misfit envelope is defined by the maximum and minimum values of the misfit at any horizontal location in space. A zero misfit throughout the depth would result in a horizontal line at zero. The top three panels show the misfit for the preferred AVW accumulation rate (Figures 10a and 10b) and for a uniform accumulation rate (Figure 10c), for which the misfit is much greater. The strong contrast between Figures 10a and 10c, with a much better fit being obtained by the physically realistic AVW accumulation rate pattern, is extremely encouraging, indicating that the method has the ability to inform about spatial accumulation-rate patterns. There is little difference between the two plots at high frequency, giving support to our assumption that the high frequency component of the misfit is due to the inadequate resolution of the BEDMAP data and to modeling errors arising from not including short-range coupling arising from higher-order mechanical effects.

[54] The breadth of the envelope has some important information; where it is narrow, the misfit sign is consistent between all the layers, and we assume that whatever caused the misfit was at least constant in time. Where the envelope is broad, other factors must come into play, and time

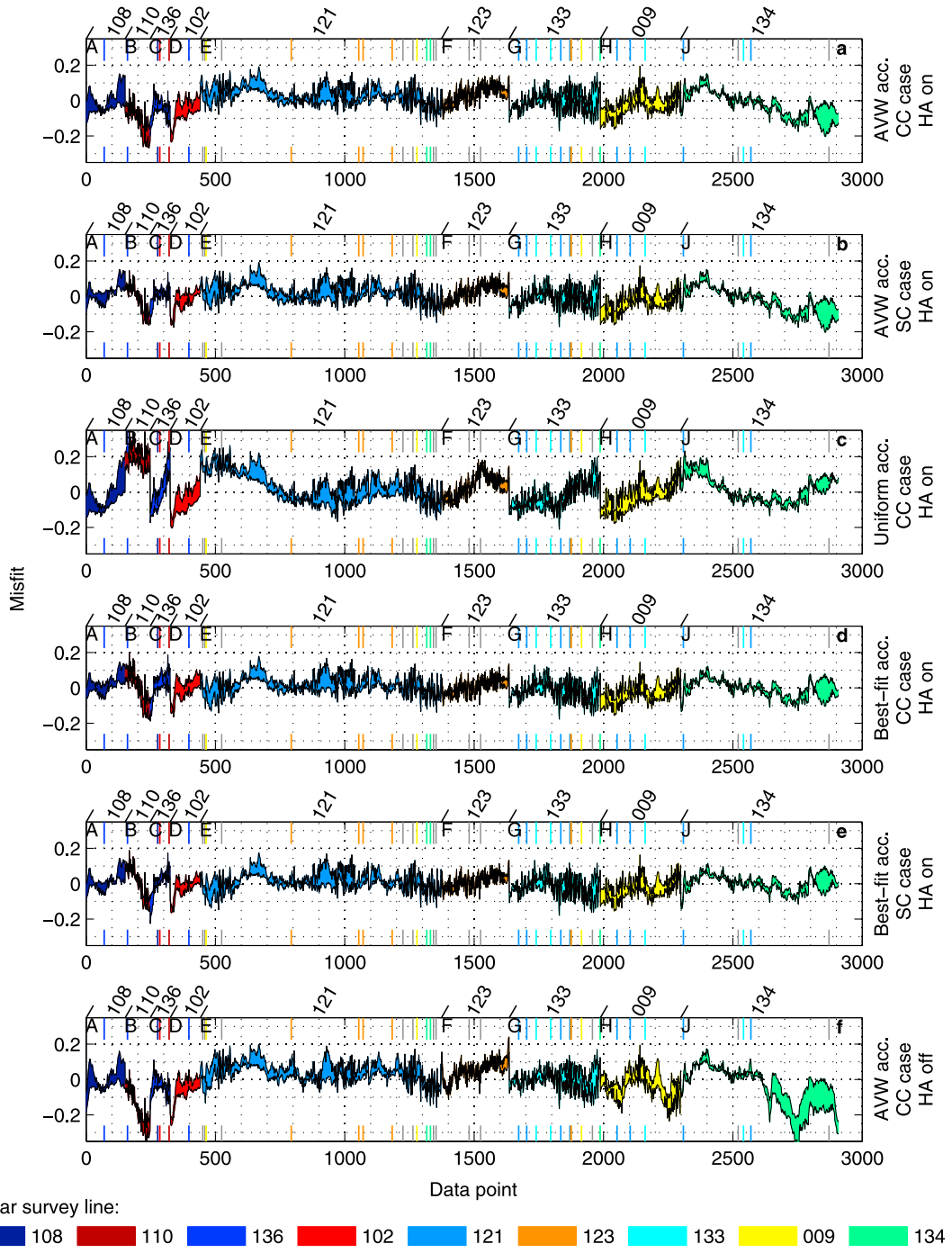

Figure 10. Plots of misfit envelope (black line) for all radar survey lines for different cases and accumulation-rate patterns. (a and b) AVW accumulation rate for CC and SC case. (c) Uniform spatial accumulation rate for CC case. (d and e) Best estimates accumulation rate for CC and SC case. (f) As in Figure 10a but with no horizontal advection. Calculations used 10 km grid, plug flow, and geothermal heat flux of 50 mW/m^2. Note that colored ticks mark position of crossovers with radar survey line of the same color. Gray ticks and labeling as in Figure 4.

dependence, presumably in the accumulation rate, is a primary suspect. Horizontal advection may also play a role. Comparing Figure 10f with Figure 10a shows that including horizontal advection improves the match. This is particularly true at the north end of Line 134 (between points 2600 and 2900), where the envelope width is much broader in the case where there is no horizontal advection. This occurs where the line intersects fast flow areas (the upper reaches of the Byrd Glacier), where horizontal advection is expected to play an important role. Along Line 009, at the grid north

end, in the Lambert Basin, there is a significant improvement from approximately 100 km away from the divide onwards, which can also be seen in Figure S3 in the auxiliary material. This observation is consistent with our understanding: horizontal advection is not generally important in divides, but clearly has an effect in ice streams, and ignoring it would affect our inferred accumulation-rate perturbation.

7.2. Tuning the Spatial Pattern in the Accumulation Rate to Improve the Match

[55] In order to assess our ability to match observed and modeled isochrone geometry, we have to recognize that there are several horizontal length scales involved in the problem. One such horizontal scale is set by the vertical scale imposed by the ice thickness (approximately 3 km), which defines a horizontal coupling length for stress effects. Further physical effects are due to the downstream propagation of perturbations in topography, flow mode, basal conditions, measured over tens to hundreds of kilometers. A further set of effects arise from the way we have carried out the surveying and the modeling: (1) the horizontal extent of correlated line set, (2) the size of the grid (5 km, 10 km and 20 km) on which the age equation is solved, and (3) the horizontal resolution of the picked lines (here, at most, twice the ice thickness), onto which the model predictions are interpolated. We now make the assumption that long (hundreds to thousands of kilometers) wavelength misfit does not arise from a cumulative effect of inadequate modeling of the flow response to short-wavelength phenomena such as basal topography, changes in flow mode etc., and that it is due to regional or continental misspecifications of the spatial accumulation-rate pattern.

[56] It is evident from Figures 8a and 8b that there is a spatial pattern in the misfit for the CC case, with, on the broad (1000 km) scale, a positive misfit near the South Pole and a negative misfit near Dome C, with a trend from south to north aligned with the South Pole/Dome C meridian. The spatial scale of this misfit is so large that it is clearly not due to topographic effects, and also seems rather larger than the flow field structures such as ice streams (100 km width). We therefore suppose that it is due to accumulation-rate misspecification. This is not equivalent to saying that modern spatial accumulation-rate patterns are wrong, only that they are unrepresentative of the time-averaged spatial accumulation-rate patterns. In fact we can make a stronger statement, because the accumulation rate derived from the 17.5 ka isochrone found in the Vostok cluster, but not in the EPICA cluster, has a very good match (Figure 4c) with the modern accumulation rate from AVW. Given the mismatch we observe on broad horizontal length scales over the whole of the time period, the modern accumulation rate is not representative of the accumulation rate averaged over periods which include glacial conditions, that is, during periods of Northern Hemisphere high latitude glaciation and expansion of ice in Antarctica.

[57] This has to be qualified somewhat, because the temporal sampling of the layers varies over the study region. Considering now layers that sample the glacial period, Figure 9, which shows the connected layer that has the lowest overall misfit (73 ka), one can see a trend of positive misfit for a zone near the South Pole, negative near Dome C, negative at Vostok and positive in the areas to the north and west of Vostok. This is very similar to the overall misfit pattern, as shown in the fence diagram Figure 8 and inspection of Figures S1 and S2, where more detailed plots are shown, shows broadly similar patterns.

[58] This indicates that modern accumulation rates are too low toward the South Pole, and too high around Dome C. The sampling at greater depth (Figure 8 and, in the auxiliary material, Figures S1 and S2, reflect this pattern, and also indicate that modern accumulation-rate patterns are too high adjacent to the Transantarctic mountains (middle to far end of radar survey line 134). This is in accordance with the findings of *Siegert et al.* [2003], which suggest that surface ablation existed in this region during the last glacial period. It should be emphasized that this is a relative pattern and does not refer to absolute values. The strongly negative zone lying at the north end (or far end, see Figure 2) of Line 110 becomes less strong with depth, over the time interval 37 ka to 72 ka (Figure 9d). This could reflect a change in spatial ice accumulation pattern. However, considering that the spatial trend of the misfit stays the same but is smaller in magnitude at depth, we note that this may also reflect compression which will reduce misfits at depth. This is true for the strain models implied by the shape functions we use.

[59] We have carried out a heuristic procedure to improve the match in order to validate our assertion that the results show that modern spatial accumulation-rate patterns are not representative of accumulation rates throughout glacial/interglacial cycles. Based on the spatial pattern of the misfit (modeled layers too shallow at South Pole compared with the observed; too deep at EPICA) a quadratic surface $\chi(x, y)$ covering the area of the picked radargrams was constructed. The accumulation rate was adjusted by adding or subtracting the accumulation rate according to $\phi\chi$, where ϕ is a multiplier. The functional form of the polynomial $\chi(x, y)$ is given in section S9, and is plotted against Antarctica in Figure S7. The multiplier ϕ was adjusted until the best fit (smallest mean square misfit) was obtained. This is not a fully flexible adjustment pattern, as the relative magnitude of the polynomial terms defining the surface was fixed and there is no real physical justification for the shape of the surface. Nevertheless it is capable of significant improvements in the match.

[60] The optimal value of ϕ was different for the CC and SC case; the total mean square misfit was reduced to 2.24×10^{-3} for the CC case and to 2.36×10^{-3} for the SC case, compared with values of 3.05×10^{-3} and 3.64×10^{-3}, respectively (see Table 3). The best fit spatial accumulation-rate patterns are shown in Figure 8c.

[61] Figure 8d shows the fence diagrams for the optimal improved match, CC case. The amplitude of the misfit is smaller, particularly in the whole EPICA cluster, Line 134 and the Vostok region. At the junction of 110 and 136 the misfit changes sign and becomes greater in magnitude.

[62] In the envelope plot (Figure 10) we compare the misfits computed with the adjusted spatial accumulation-rate patterns (Figures 10d and 10e) with the modern pattern (Figure 10a). By adjusting the accumulation rate over long wavelengths to minimize the misfit we have successfully reduced trends over the individual lines. These adjustments have not in general affected the breadth of the misfit envelope, but do act to reduce the mean value of the misfit.

[63] The tuned mean accumulation rates reflect the way the layers sample over glacials and interglacials. By looking at Figure 2 it is clear that the sampling of age varies in space. Around Vostok, there is sampling from 17.5 ka to 170.5 ka; around EPICA there is sampling between 37 ka and 352.5 ka. However, near the South Pole there are only layers sampling from 17.5 ka to 73.5 ka. The trend we imposed to obtain a match may be biased by the variation in temporal sampling intervals at each of the different areas. However, if there is a binary state in glacial/interglacial climate [e.g., *Stocker and Wright*, 1991], with corresponding spatial accumulation-rate patterns, then the tuned accumulation-rate pattern, although it samples both glacial and interglacial, will reflect glacial conditions primarily as a consequence of the greater number of layers found in ice from this climate state. Some of these issues can be resolved by a time-dependent model.

[64] We cannot rule out that some of the mismatch might arise from significant changes in the spatial organization of the flow of East Antarctic ice sheet, which would likely be associated with changes in its geometry. The more conservative hypothesis is that the changes are associated with the known changes in climate. Time-dependent modeling is needed to resolve these issues.

8. Conclusions

[65] It has been known for a long time that the accumulation rate measured over time from ice cores changes from glacial to interglacial periods. Our analysis has shown something more; that the spatial pattern also changes with time. The fact that where we have been able to derive postglacial accumulation rates and show that they correspond well with modern accumulation rates over substantial areas considerably strengthens our ability to make statements about accumulation rates during the last glacial period and earlier periods.

[66] We have created a three-dimensional balance velocity model of ice flow in Antarctica which has been used to compute temperature and age fields as a function of vertical and horizontal position in the ice. It yields basal temperatures which have been used to compute melt rates. This model is steady but can be used to calculate isochrone geometry under the less restrictive assumption that relative patterns of accumulation rate do not change over time. This model can then be used to explore hypotheses about changes in the spatial pattern by comparing modern accumulation-rate patterns with those inferred from tuning exercises.

[67] The steady assumption means that the temperature fields are probably unrealistic as they do not reflect changes in ice thickness or ice upper surface temperatures during ice age cycles. Nevertheless, by performing a sensitivity study on thermal parameters, we showed that isochrone geometry is not very sensitively dependent on the flow changes caused by changes in the temperature field, at least in the central areas where many observations of layers have been made.

[68] Using radar layers picked from the SPRI-NSF-TUD lines we evaluated the match between observed and computed isochrone elevation. We found that ignorance of the geothermal heat flux is not a strong obstacle to matching the data. The changes in misfit induced by varying the parameters in the thermal sensitivity studies are two orders of magnitude smaller than typical misfits. Including horizontal advection is important even in slow flowing areas in the center of East Antarctica.

[69] The short-scale misfits caused by using over-simplified mechanical models seem to average out, and do not significantly affect trends over long distances. Models that rely on vertical flow only do not explain all features of the flow and approaches such as [e.g., *Siegert et al.*, 2003] (plane flow) and the three-dimensional approach in this paper are necessary.

[70] We found a long wavelength misfit which we attributed to a misspecification of the time-averaged spatial accumulation-rate pattern, and showed that the misfit could be reduced by altering this pattern. To go further in quantifying this requires a properly time-dependent model, and will form the basis of future work.

[71] In terms of future surveying and modeling strategies for determining accumulation-rate records, one might feel that groupings of lines are good, particularly those that permit long-distance correlations to be established. The sampling of local patterns and more regional patterns with spacings of 100 km are useable and may even be close to optimal for looking at long-range spatial changes in accumulation rate, provided that layers can be correlated at crossovers. Overly close sampling is simply contaminated by the basal topography. It seems that for the purposes of understanding spatial accumulation-rate patterns having lines directly along and across flow is not an important issue provided a three-dimensional model is used. This may not be true for fast flow areas.

[72] Apart from the obvious issue of incorporating more data as and when it becomes available, direct modeling of changes in accumulation-rate pattern over time is the obvious next step. We think that this could profitably be done by extending the balance velocity mode used in this paper but with a prescribed changing topography, rather than proceeding directly to full three-dimensional models [*Ritz et al.*, 2001; *Huybrechts et al.*, 2007; *Pollard and DeConto*, 2009].

[73] **Acknowledgments.** We would like to thank three anonymous reviewers for thorough reviews improving the manuscript. Funding for work leading to this paper was provided by the U.K. Natural Environment Research Council grant NER/A/S/2001/01011. G. Leysinger Vieli is currently funded by a Royal Society BP Dorothy Hodgkin Fellowship.

References

Arthern, R. J., D. G. Vaughan, and D. Winnebrenner (2006), Antarctic snow accumulation mapped using polarization of 4.3-cm wavelength microwave emission, *J. Geophys. Res.*, *111*, D06107, doi:10.1029/2004JD005667.

Bamber, J. L., J. L. Bamber, D. G. Vaughan, and I. R. Joughin (2000), Widespread complex flow in the interior of the Antarctic ice sheet, *Science*, *287*, 1248–1250.

Bell, R. E., M. Studinger, A. A. Tikku, G. K. C. Clarke, M. M. Gutner, and C. Meertens (2002), Origin and fate of Lake Vostok water frozen to the base of the East Antarctic ice sheet, *Nature*, *416*, 307–310.

Bingham, R. G., M. J. Siegert, D. A. Young, and D. D. Blankenship (2007), Organized flow from the South Pole to the Filchner-Ronne ice shelf: An assessment of balance velocities in interior East Antarctica using radio echo sounding data, *J. Geophys. Res.*, *112*, F03S26, doi:10.1029/2006JF000556.

Budd, W. F., and R. C. Warner (1996), A computer scheme for rapid calculations of balance-flux distributions, *Ann. Glaciol.*, *23*, 21–27.

Carter, S. P., D. A. Blankenship, D. D. Young, and J. W. Holt (2009), Using radar-sounding data to identify the distribution and sources of subglacial water: Application to Dome C, East Antarctica, *J. Glaciol.*, *55*, 1025–1040.

Dahl-Jensen, D., N. Gundestrup, S. P. Gogineni, and H. Miller (2003), Basal melt at NorthGRIP modeled from borehole, ice-core and radio-echo sounder observations, *Ann. Glaciol.*, *37*, 207–212.

Drewry, D. J., and D. T. Meldrum (1978), Antarctic airborne radio echo sounding, 1977-78, *Polar Rec.*, *19*, 267–278.

Eisen, O. (2008), Inference of velocity pattern from isochronous layers in firn, using an inverse method, *J. Glaciol.*, *54*, 613–630.

Fahnestock, M., W. Abdalati, I. Joughin, J. Brozena, and P. Gogineni (2001), High geothermal heat flow, basal melt, and the origin of rapid ice flow in central Greenland, *Science*, *294*, 2338–2342, doi:10.1126/science.1065370.

Fox Maule, C., M. E. Purucker, N. Olsen, and K. Mosegaard (2005), Heat flux anomalies in Antarctica revealed by satellite magnetic data, *Science*, *309*, 464–467.

Fujita, S., H. Maeno, S. Uratsuka, T. Furukawa, S. Mae, Y. Fujii, and O. Watanabe (1999), Nature of radio echo layering in the Antarctic ice sheet detected by a two-frequency experiment, *J. Geophys. Res.*, *104*, 13,013–13,024, doi:10.1029/1999JB900034.

Fowler, A. C. (1992), Modelling ice sheet dynamics, *Geophys. Astrophys. Fluid Dyn.*, *63*, 29–65.

Hempel, L., F. Thyssen, N. Gundestrup, H. B. Clausen, and H. Miller (2000), A comparison of radio-echo sounding data and electrical conductivity of the GRIP ice core, *J. Glaciol.*, *46*, 369–374.

Hindmarsh, R. C. A. (1997), Use of ice-sheet normal modes for initialization and modelling small changes, *Ann. Glaciol.*, *25*, 85–96.

Hindmarsh, R. C. A., G. J.-M. C. Leysinger Vieli, M. J. Raymond, and G. H. Gudmundsson (2006), Draping or overriding: The effect of horizontal stress gradients on internal layer architecture in ice sheets, *J. Geophys. Res.*, *111*, F02018, doi:10.1029/2005JF000309.

Hindmarsh, R. C. A., G. J.-M. C. Leysinger Vieli, and F. Parrenin (2009), A large-scale numerical model for computing isochrone geometry, *Ann. Glaciol.*, *50*, 130–140.

Hodgkins, R., M. J. Siegert, and J. A. Dowdeswell (2000), Geophysical investigations of ice-sheet internal layering and deformation in the Dome C region of central East Antarctica, *J. Glaciol.*, *46*, 161–166.

Huybrechts, P., O. Rybak, F. Pattyn, U. Ruth, and D. Steinhage (2007), Ice thinning, upstream advection, and non-climatic biases for the upper 89% of the EDML ice core from a nested model of the Antarctic ice sheet, *Clim. Past*, *3*, 577–589.

Le Brocq, A. M., A. J. Payne, and M. J. Siegert (2006), West Antarctic balance calculations: Impact of flux-routing algorithm, smoothing algorithm and topography, *Comput. Geosci.*, *32*, 1780–1795.

Lemieux-Dudon, B., E. Blayo, J.-R. Petit, C. Waelbroeck, A. Svensson, C. Ritz, J.-M. Barnola, B. M. Narcisi, and F. Parrenin (2010), Consistent dating for Antarctica and Greenland ice cores, *Quat. Sci. Rev.*, *29*, 8–20.

Leonard, K., R. E. Bell, M. Studinger, and B. Tremblay (2004), Anomalous accumulation rates in the Vostok ice-core resulting from ice flow over Lake Vostok, *Geophys. Res. Lett.*, *31*, L24401, doi:10.1029/2004GL021102.

Leysinger Vieli, G. J.-M. C., M. J. Siegert, and A. J. Payne (2004), Reconstructing ice-sheet accumulation rates at ridge B, East Antarctica, *Ann. Glaciol.*, *39*, 326–330.

Leysinger Vieli, G. J.-M. C., R. C. A. Hindmarsh, and M. J. Siegert (2007), Three-dimensional flow influences on radar layer stratigraphy, *Ann. Glaciol.*, *46*, 22–28.

Llubes, M., C. Lanseau, and F. Rémy (2006), Relations between basal condition, sublacial hyrological networks and geothermal flux in Antarctica, *Earth Planet. Sci. Lett.*, *241*, 655–662.

Lythe, M. B., D. G. Vaughan, and the BEDMAP Consortium (2001), BEDMAP: A new ice thickness and subglacial topographic model of Antarctica, *J. Geophys. Res.*, *106*, 11,335–11,351, doi:10.1029/2000JB900449.

Martín, C., R. C. A. Hindmarsh, and F. J. Navarro (2006), Dating ice flow change near the flow divide at Roosevelt Island, Antarctica, by using a thermomechanical model to predict radar stratigraphy, *J. Geophys. Res.*, *111*, F01011,doi:10.1029/2005JF000326.

Neal, C. S. (1976), Radio-echo power profiling, *J. Glaciol.*, *17*, 527–530.

Nereson, N. A., and C. F. Raymond (2001), The elevation history of ice streams and the spatial accumulation pattern along the Siple Coast of West Antarctica inferred from ground-based radar data from three inter-ice-stream ridges, *J. Glaciol.*, *47*, 303–313.

Nereson, N. A., C. F. Raymond, E. D. Waddington, and R. W. Jacobel (1998), Migration of the Siple Dome ice divide, West Antarctica, *J. Glaciol.*, *44*, 643–652.

Nereson, N. A., C. F. Raymond, R. W. Jacobel, and E. D. Waddington (2000), The accumulation pattern across Siple Dome, West Antarctica, inferred from radar-detected internal layers, *J. Glaciol.*, *46*, 75–87.

Nye, J. F. (1963), Correction factor for accumulation measured by the thickness of the annual layers in an ice sheet, *J. Glaciol.*, *4*, 785–788.

Parrenin, F., and R. C. A. Hindmarsh (2007), Influence of a non-uniform velocity field on isochrone geometry along a steady flowline of an ice sheet, *J. Glaciol.*, *53*, 612–622.

Parrenin, F., J. Jouzel, C. Waelbroeck, C. Ritz, and J.-M. Barnola (2001), Dating the Vostok ice core by an inverse method, *J. Geophys. Res.*, *106*, 31,837–31,851.

Parrenin, F., R. C. A. Hindmarsh, and F. Rémy (2006), Analytical solutions for the effect of topography, accumulation rate variations and flow divergence on isochrone layer geometry, *J. Glaciol.*, *52*, 191–202.

Parrenin, F., et al. (2007), The EDC3 chronology for the EPICA Dome C ice core, *Clim. Past*, *3*, 485–497.

Pollard, D., and R. M. DeConto (2009), Modelling West Antarctic ice sheet growth and collapse through the past five million years, *Nature*, *458*, 329–332, doi:10.1038/nature07809.

Pattyn, F. (2010), Antarctic subglacial conditions inferred from a hybrid ice sheet/ice stream model, *Earth Planet. Sci. Lett.*, *295*, 451–461, doi:10.1016/j.epsl.2010.04.025.

Ritz, C., V. Rommelaere, and C. Dumas (2001), Modeling the evolution of Antarctic ice sheet over the last 420,000 years: Implications for altitude changes in the Vostok region, *J. Geophys. Res.*, *106*, 31,943–31,964.

Robin, G. Q., D. J. Drewry, and D. T. Meldrum (1977), International studies of ice sheet and bedrock, *Philos. Trans. R. Soc. London, Ser. B*, *279*, 185–196.

Ruddiman, W. F., and M. E. Raymo (2003), A methane-based time scale for Vostok ice, *Quat. Sci. Rev.*, *22*, 141–155.

Shapiro, N. M., and M. H. Ritzwoller (2004), Inferring surface heat flux distributions guided by a global seismic model: Particular application to Antarctica, *Earth Planet. Sci. Lett.*, *223*, 213–224.

Siegert, M., and J. Ridley (1998), An analysis of the ice-sheet surface and subsurface topography above the Vostok Station subglacial lake, central East Antarctica, *J. Geophys. Res.*, *103*, 10,195–10,207.

Siegert, M. J., R. C. A. Hindmarsh, and G. S. Hamilton (2003), Evidence for a large surface ablation zone in central East Antarctica during the last ice age, *Quat. Res.*, *59*, 114–121.

Siegert, M. J., B. Welch, D. Morse, A. Vieli, D. D. Blankenship, I. Joughin, E. C. King, G. J.-M. C. Leysinger Vieli, A. J. Payne, and R. Jacobel (2004a), Ice flow direction change in interior West Antarctica, *Science*, *305*, 1948–1951, doi:10.1126/science.1101072.

Siegert, M. J., R. Hindmarsh, H. Corr, A. Smith, J. Woodward, E. C. King, A. J. Payne, and I. Joughin (2004b), Subglacial Lake Ellsworth: A candidate for in situ exploration in West Antarctica, *Geophys. Res. Lett.*, *31*, L23403, doi:10.1029/2004GL021477.

Stocker, T. F., and D. G. Wright (1991), Rapid transitions of the oceans deep circulation induced by changes in surface-water fluxes, *Nature*, *351*, 729–732.

Turchetti, S., K. Dean, S. Naylor, and M. J. Siegert (2008), Accidents and opportunities: a history of the radio echo-sounding of Antarctica, 1958–79, *Br. J. Hist. Sci.*, *41*, 417–444, doi:10.1017/S0007087408000903.

Vaughan, D. G., J. L. Bamber, M. Giovinetto, J. Russell, and A. P. R. Cooper (1999), Reassessment of net surface mass balance in Antarctica, *J. Clim.*, *12*, 933–946.

Waddington, E. D., T. A. Neumann, M. R. Koutnik, H. P. Marshall, and D. L. Morse (2007), Inference of accumulation-rate patterns from deep layers in glaciers and ice sheets, *J. Glaciol.*, *53*, 694–712.

Whillans, I. M. (1976), Radio-echo layers and the recent stability of the West Antarctic ice sheet, *Nature*, *264*, 152–155, doi:10.1038/264152a0.

S. Bo, Polar Research Institute of China, 451 Jinqiao Rd., Pudong, Shanghai 200136, China. (sunbo@pric.gov.cn)

R. C. A. Hindmarsh, Physical Sciences Division, British Antarctic Survey, Natural Environment Research Council, High Cross, Madingley Road, Cambridge CB3 0ET, UK. (rcah@bas.ac.uk)

G. J.-M. C. Leysinger Vieli, Department of Geography, Durham University, Science Laboratories, South Road, Durham DH1 3LE, UK. (g.j.m.c.leysinger-vieli@durham.ac.uk)

M. J. Siegert, School of GeoSciences, Grant Institute, University of Edinburgh, West Mains Road, Edinburgh EH9 3JW, Scotland. (m.j.siegert@ed.ac.uk)